Eur. Phys. J. B **54**, 479–484 (2006)
DOI: 10.1140/epjb/e2007-00018-6

THE EUROPEAN PHYSICAL JOURNAL B

Size effect on alloying ability and phase stability of immiscible bimetallic nanoparticles

S. Xiao, W. Hu[a], W. Luo, Y. Wu, X. Li, and H. Deng

Department of Applied Physics, Hunan University, 410082 Changsha, P.R. China

Received 12 September 2006 / Received in final form 19 December 2006
Published online 17 January 2007 –

Abstract. In the present paper, the surface and size effects on the alloying ability and phase stability of immiscible alloy nanoparticles have been studied with calculating the heats of formation of Au-Pt alloy nanoparticles from the single element nanoparticles of their constituents (Au and Pt) with a simple thermodynamic model and an analytic embedded atom method. The results indicated that, besides the similar compositional dependence of heat of formation as in bulk alloys, the heat of formation of alloy nanoparticles exhibits notable size-dependence, and there exists a competition between size effect and compositional effect on the heat of formation of immiscible system. Contrary to the positive heat of formation for bulk-immiscible alloys, a negative heat of formation may be obtained for the alloy nanoparticles with a small size or dilute solute component, which implies a promotion of the alloying ability and phase stability of immiscible system on a nanoscale. The surface segregation results in an extension of the size range of particles with a negative heat of formation. The molecular dynamics simulations have indicated that the structurally and compositionally homogeneous AuPt nanoparticles tend to form a core-shell structure with temperature increasing.

PACS. 61.46.-w Nanoscale materials – 64.75.+g Solubility, segregation, and mixing; phase separation

1 Introduction

In the past decades, the studies on metallic nanoparticles have attracted a lot of interest because of their scientific significance and prospective applications. Relative to bulk materials, the most important characteristic of nanoparticles is their size effect [1–3]. In the small size range, the metallic nanoclusters present competitive structural motifs, such as icosahedron, decahedron, truncated octahedron [1,4,5]. Contrasting to homogeneous nanoparticles composed of only one type of atom, the alloy nanoparticles exhibit more complicated structure and some special physical and chemical properties as a result of alloying effect [6–9]. For example, in many systems, the bimetallic nanoparticles can be formed with a core-shell structure [6,10,11]. Recently, the enhanced bifunctional catalytic properties of bimetallic nanoparticles have made them attractive in the field of chemical catalysis [12].

Driven by high surface-to-volume ratio and surface free energy, the nanoparticles have a strong tendency of coalescence even at much lower temperatures than their melting temperatures as they are put together [13]. This feature are early expected to be applied in the alloying of components which are immiscible in the solid and/or molten state [14]. As known from the Au-Pt alloy phase diagram, there exists a miscible gap for Au-Pt bulk alloy [15]. However, the Au-Pt alloy nanoparticles with several nanometers can be synthesized chemically almost in the entire composition range [16], which demonstrates that the alloying mechanism and phase properties of nanoscale materials are evidently different from those of bulk crystalline state. For instance, Shibata et al. interpreted the size-dependent spontaneous alloying of Au-Ag nanoparticles under the framework of defect enhanced diffusion [17]. Boyen et al. found that the closed packed full-shell clusters containing 55 Au atoms exhibit an outstanding stability against alloying in Au-In system [18]. At present, on the study of the alloying behavior of nanoparticles, more attention has been paid to the evolution of microstructure. To the best of our knowledge, there is little report on the alloying thermodynamics and phase stability of bimetallic nanoparticle, especially for the immiscible ones. Christensen et al. studied the effect of cluster size on phase separation in the interior of a bimetallic alloy cluster using a Monte Carlo simulation [19]. Although Liang et al. calculated the size-dependent formation enthalpy of MgH_2 and SnTe nanoparticles [20], they only considered the surface effect against the corresponding bulk materials. In this work, by calculating the heat of formation of

[a] e-mail: wangyuhu2001cn@yahoo.com.cn

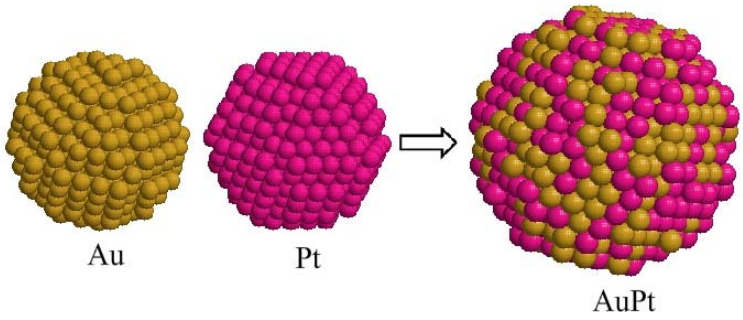

Fig. 1. (Color online) The schematic diagram for the initial configuration of an AuPt alloy nanoparticle.

Au-Pt nanoparticles from their monometallic ones using a thermodynamic model and an analytic embedded atom method (AEAM), we have analyzed the surface and size effects on alloying ability and phase stability of immiscible binary alloy on a nanometer scale, which is of importance for the study of alloying thermodynamics of nanoparticles and the fabrication of immiscible alloys.

2 Theory and method

Although the core-shell structure occurs in many nanoalloy systems, here we mainly consider the structurally and compositionally homogeneous system. Figure 1 illustrates a schematic diagram for the initial configuration of an AuPt alloy nanoparticles. According to the definition of heat of formation being the energy change associated with the formation of alloy from its constituent metals, the heat of formation of alloy nanoparticle from the pure nanoparticles of their constituents can be expressed as

$$E_f^{pA\text{-}B} = E_c^{pA\text{-}B} - (1-x)E_c^{pA} - xE_c^{pB} \tag{1}$$

where the superscripts A-B, A and B denote alloy and its constituent elements A and B, respectively. x is the chemical concentration of the element B in alloy nanoparticles. E_c^p is the mean atomic cohesive energy of nanoparticles. The size-dependent cohesive energy of nanoparticles has the following expression [3]:

$$E_c^p = E_c^b\left(1 - \frac{d}{D}\right) \tag{2}$$

where E_c^b is the cohesive energy of the corresponding bulk material. d and D represent the diameters of a single atom and spherical nanoparticle, respectively. For alloy nanoparticle, d denotes the mean atomic diameter derived from Vegard's law. If neglecting the minor difference of atomic volume for atoms resided in the interior of and on the surface layer of spherical nanoparticles, there exists a relation among d, D and the number of atoms (N) in a nanoparticle as follows

$$\frac{d}{D} = \sqrt[3]{\frac{1}{N}}. \tag{3}$$

If the formed alloy nanoparticles have the same structure as that of a homogeneous disordered solid solution, substituting equations (2) and (3) into equation (1) yields

$$E_f^{pA\text{-}B} = E_c^{bA\text{-}B}\left(1 - \sqrt[3]{\frac{1}{N}}\right) - (1-x)E_c^{bA}\left(1 - \sqrt[3]{\frac{1}{N(1-x)}}\right) - xE_c^{bB}\left(1 - \sqrt[3]{\frac{1}{Nx}}\right) \tag{4}$$

one can find that, to obtain the heat of formation of an alloy nanoparticle from the single element nanoparticles of its constituents, it is only needed to calculate the cohesive energy of the corresponding bulk alloy. However, it is important to notice that equation (4) is not suitable for alloy nanoparticles with a core-shell structure since where only partial alloying exists at interface.

In the present AEAM scheme [21,22], the cohesive energy of a disordered solid solution can be written as

$$E_c^{bA\text{-}B} = \left[\frac{1}{2}\phi^A(r) + F^A(\rho) + M^A(P)\right](1-x) + \left[\frac{1}{2}\phi^B(r) + F^B(\rho) + M^B(P)\right]x \tag{5}$$

where $\phi(r)$, $F(\rho)$ and $M(P)$ are the pair potential as a function of distance between atoms, embedding energy and modified term, respectively. $\rho(r)$ is electron density and $P(r)$ is the second order item of electron density. The two-body potential between two different species of atom A and B is included in the terms of $\phi^A(r)$ and $\phi^B(r)$. A detail description on each item can be found in references [21] and [22]. All the model parameters, determined from fitting physical attributes such as lattice parameter, cohesive energy, vacancy formation energy and elastic constants for Au, Pt and Au-Pt intermetallic compound, are listed in Table 1. In the AEAM, since the embedding energy and modified term are assumed to be independent of the source of the electron density, their expressions in alloy systems still follow monatomic forms. To describe the pairwise interaction between heterogeneous atoms, here an adjustable parameter μ is introduced in

Table 1. AEAM model parameters for Au, Pt and Au-Pt.

Parameter	Au	Pt	AuPt
n	1.41	1.43	
F_0 (eV)	2.969	4.403	
α (10^{-5} eV)	–4.968	–7.447	
k_{-1} (eV)	54.351	98.633	
k_0 (eV)	–25.416	–46.656	
k_1 (eV)	–19.380	–31.402	
k_2 (eV)	–2.223	–13.393	
k_3 (eV)	0.573	10.527	
k_4 (eV)	–8.037	–17.908	
f_e (eV/Å^3)	3.87	5.64	
r^p (Å)	2.900	2.834	
μ			1.14

alloy potential. Figure 2a shows the formation enthalpy of Au-Pt disordered solid solution from the present model together with other calculated [23–25] and experimental values [26]. The results have a good agreement with experiment and other calculations, which indicates that the adopted AEAM model is reliable.

3 Results and discussion

Figure 2b shows the variation of the heat of formation of Au-Pt alloy nanoparticles with Pt atomic concentration for several samples with indicated total number of atoms (i.e. particle size). Naturally, as a result of alloying effect, the heat of formation of alloy nanoparticles shows a similar compositional dependence as in bulk materials. Comparing with bulk alloys, the most prominent characteristic on the heat of formation of nanoparticles is its size-dependence. At a fixed Pt atomic concentration, the heat of formation decreases with the alloy particle size decreasing, and its value may turn from positive to negative. This differs from the size-dependent formation enthalpy calculated by Liang et al. [20], where they only considered surface effect relative to the corresponding bulk materials. As the number of atoms in Au-Pt alloy nanoparticles not exceeding 7000 (about 6 nm in diameter of spherical particle), the heat of formation within full concentration region of Pt ($0 < x < 1$) is negative as a result of surface effect, which indicates that the the alloying of Au and Pt nanoparticles becomes easy from the thermodynamic point of view, and at the same time, indicates that the Au-Pt alloy nanoparticles within this size range having a better thermodynamic stability. In addition, the heat of formation of bulk alloy has a great influence on that of nanoparticles. As shown in Figure 2b, the heat of formation in Au-rich range for Au-Pt bulk alloy is lower than that in Pt-rich one. This difference is magnified in nanoparticles. Thus, in the Au-rich range, the Au-Pt nanoparticles show negative heat of formation in a broad concentration range and a large particle size range, that is to say, the easy alloying region is extended. In Figure 3, the contour of heat of formation of disordered Au-Pt nanoparticles is shown as a function of alloy nanoparticle size and the chemical concentration of Pt atom. For

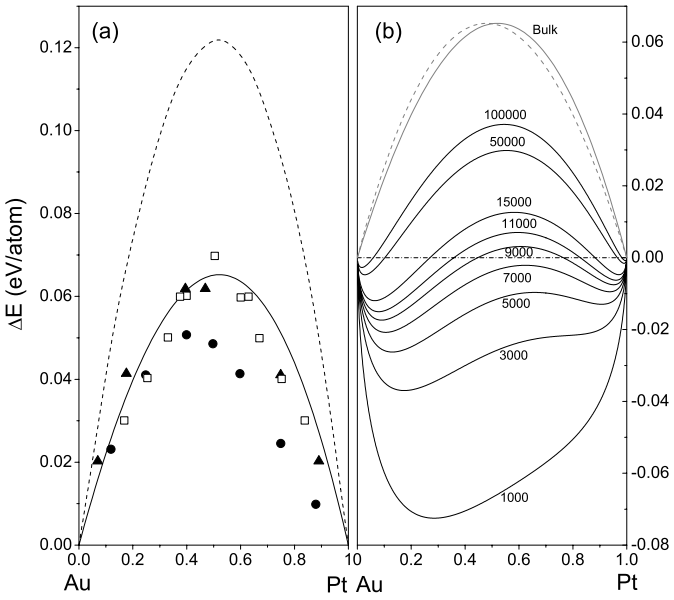

Fig. 2. (a) The heat of formation of Au-Pt disordered solid solution as a function of Pt concentration. The solid line is the corresponding result from the present calculation; dash line and full circles present the results based on old EAM (Ref. [23]) and LMTO (Ref. [24]) respectively; open squares denote the calculation from Miedema theory (Ref. [25]); full triangles denote the experimental data of Ref. [26]. (b) The variation of heat of formation for Au-Pt nanoparticles of disordered structure along with Pt concentration at several indicated number of atoms in alloy nanoparticles. The dash line denotes the mirror-image curve of that for bulk heat of formation about the axis of $x = 0.5$, which gives a clear comparison between the heat of formation of Au-Pt along with Au and Pt concentration.

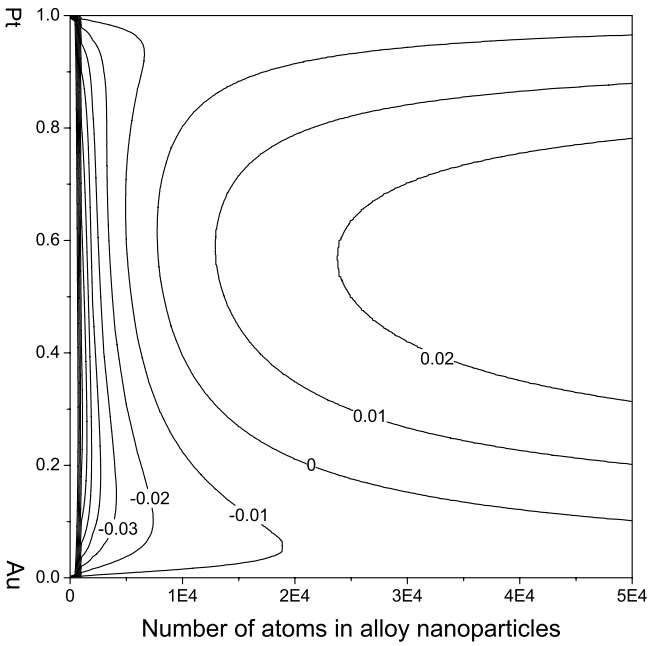

Fig. 3. The contour of heat of formation for disordered Au-Pt nanoparticles as a function of the size of alloy nanoparticles and the chemical concentration of Pt atom. The interval of energy between two adjacent contour lines is 0.01 eV.

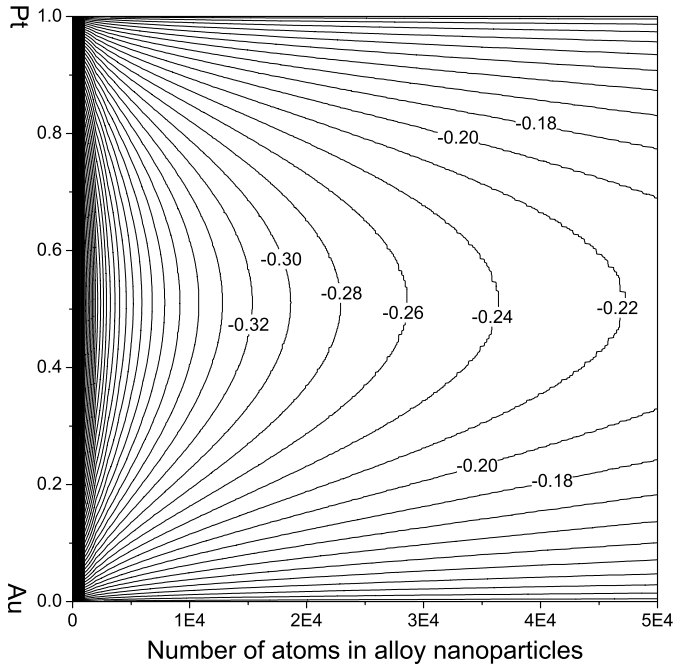

Fig. 4. The contour of the change of surface area after alloying as a function of alloy nanoparticle size and the chemical concentration of Pt atom under the hypothesis of neglecting surface relaxation and the disorered alloy obeying Vegard's law. The difference of surface area between two adjacent contour lines is 0.02 Å^2.

the nanoparticles with a dilute solute of Pt in Au or Au in Pt, there exists a broad size range in which the alloy nanoparticles exhibit negative heat of formation. This can be looked as the instability of small size particles relative to large ones.

As discussed above, the main difference between bulk materials and nanoparticles is the remarkable surface effect of the nanoparticles. Figure 4 shows the change of systematic surface area before and after alloying process under ideal condition (spherical nanoparticles without surface relaxation). Naturally, when the size of an alloy particle is fixed, there is a maximal reduction of surface area for the alloying of two equal-volume single element nanoparticles. However, comparing Figure 3 with 4, one can find that there is maximal reduction in surface area after the alloying of two isolated Au and Pt nanoparticles with approximately equal number of atoms, but on the contrary, the heat of formation is the largest. This is because there exists a competition between surface effect and alloying effect on heat of formation during alloying process for the immiscible nanoparticles.

In addition, since the surface energy of Au (1.50 J/m^2) is lower than that of Pt (2.48 J/m^2) [25], there is a thermodynamic driving force for Au atoms segregating to surface [27]. The segregation behavior in alloy nanoparticles generally induces a core-shell structure. Here we ignore the difference of structural details resulted by surface segregation. According to the effect of segregation being decreasing the systematic free energy, simply, a segregation factor f_{seg} is introduced to describe the change of cohesive energy, i.e.

$$E_c^{bA\text{-}B}(\text{Segregation}) = f_{seg} \cdot E_c^{bA\text{-}B}(\text{Ideal}). \qquad (6)$$

Figure 5 shows the variation of heat of formation for Au-Pt alloy nanoparticles with different f_{seg}. Comparing with the heat of formation of ideal alloy nanoparticles as shown in Figure 3, the effect of surface segregation is extending the size range of alloy nanoparticles with negative heat of formation. As the segregation factor f_{seg} increases from 1.001 to 1.008, the size of alloy nanoparticle, with negative formation heat in entire composition range, increases from about 7 nm to 14 nm (number of atoms from 10^4 to 10^5).

To further discuss the thermal stability of AuPt alloy nanoparticles, we have selected a specimen and used a molecular dynamics (MD) simulation to investigate its structural evolution with temperature. The considered alloy nanoparticle consists of 1055 atoms (453 Au and 602 Pt). Its initial structure (as shown in Fig. 1) is the same as that of a homogeneous disordered solid solution and annealed fully at 200 K. The details on MD description can be found in reference [28].

Figure 6 shows the structural and energetic evolution of the alloy nanoparticles in the course of heating. We can see that the specimen melts at the temperature between 1300 and 1400 K, which is evidently below the melting temperature of bulk alloy with corresponding composition. The main causation for this is the high surface to volume ratio for small particles, which as a consequence of the improved free energy at the particle surface generally results in a decrease of the melting temperature [1,28–30]. Moreover, during heating we have observed the atomic distribution (i.e. number density) around the center of mass of alloy nanoparticle, which are shown in Figure 7. At low temperature, the alloy nanoparticles keep a homogeneous structure either in its core or at surface layer. With temperature increasing, the surface segregation of Au enhances. After the alloy nanoparticle melts, almost all the Au atoms segregate to surface and the nanodroplet exhibits a core-shell structure. These indicate that although the Au and Pt can form alloy nanoparticle at small size in the entire composition range [16], the homogeneous AuPt alloy nanoparticles have a trend to decompose into a core-shell structure as temperature increasing.

4 Conclusion

In summary, using a thermodynamic model and AEAM, we have calculated the heat of formation of disordered Au-Pt alloy nanoparticles from the pure nanoparticles of their constituents. On a nanoscale, besides structural effect and alloy composition, the particle size has a great influence on the heat of formation of immiscible system. For small size alloy particles, they exhibit a negative heat of formation. The remarkable surface effect is one of the main factors that promote alloying process. As temperature increases, the structurally and compositionally homogeneous alloy

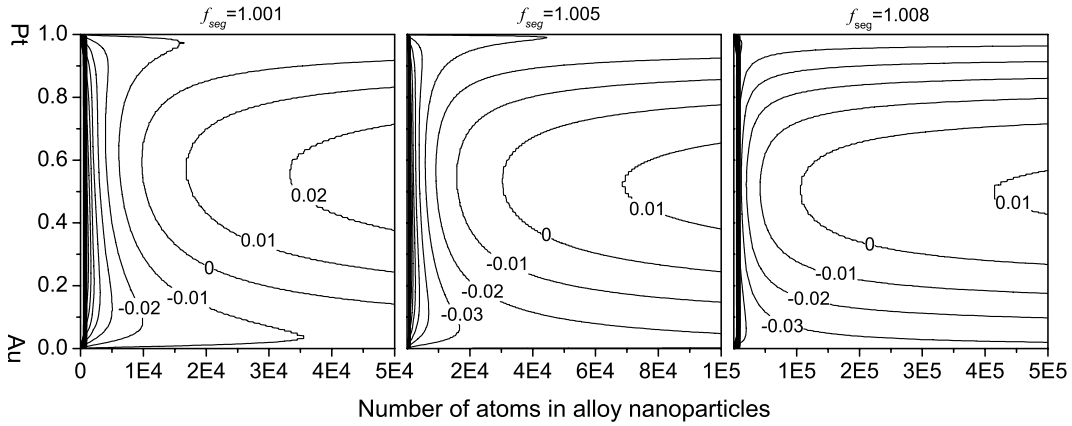

Fig. 5. The effect of surface segregation on the heat of formation of alloy nanoparticles. The interval of energy between two adjacent contour lines is 0.01 eV.

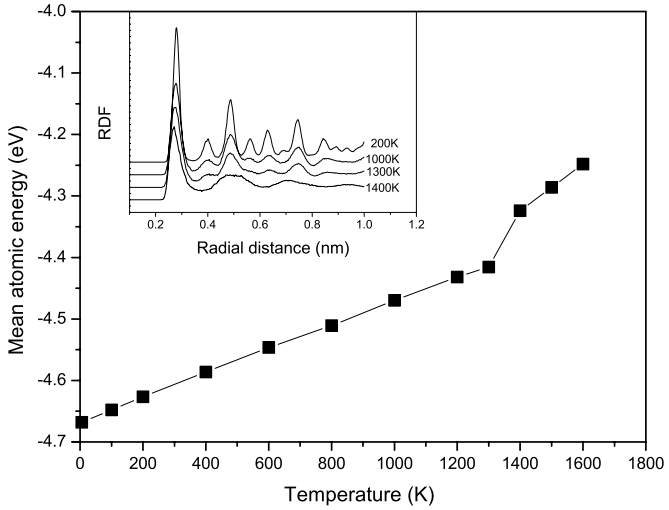

Fig. 6. The mean atomic energy as a function of temperature during heating. The insert figure shows the evolution of systematic RDF before and after melting.

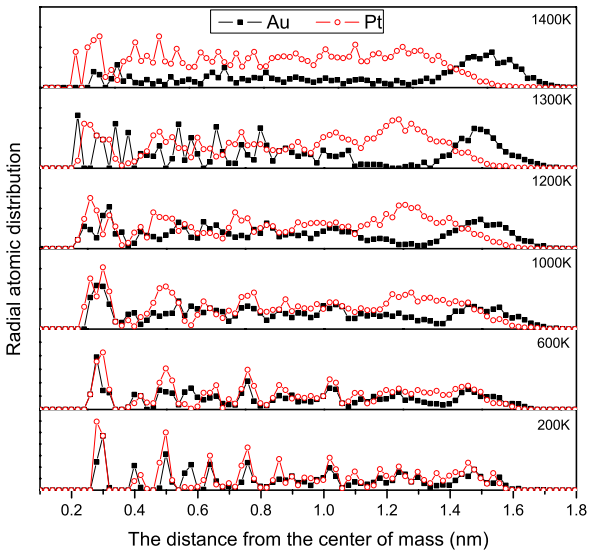

Fig. 7. (Color online) The atomic distribution around the center of mass in an alloy nanoparticle during heating.

nanoparticles tend to form a core-shell structure as a result of surface segregation. With the grain size increasing, the particles have positive heat of formation as that of bulk alloy. The surface segregation results in the extension of size- and composition-range for alloy particles with negative heat of formation. This should be a main reason why the core-shell structure occurs in many nanoalloy systems.

This work is financially supported by the NSFC (No.50371026, 50571036 and 50671035), the Hunan Provincial Natural Science Foundation, and the High Performance Computing Center of Hunan University.

References

1. F. Baletto, R. Ferrando, Rev. Mod. Phys. **77**, 371 (2005)
2. B. Balamurugan, T. Maruyama, Appl. Phys. Lett. **87**, 143105 (2005)
3. W.H. Qi, M.P. Wang, J. Mater. Sci. Lett. **21**, 1743 (2002)
4. C.L. Cleveland, U. Landman, T.G. Schaaff, M.N. Shafigullin, Phys. Rev. Lett. **79**, 1873 (1997)
5. Z. Zhang, W. Hu, S. Xiao, Phys. Rev. B **73**, 125443 (2006)
6. G. Rossi, A. Rapallo, C. Mottet, A. Fortunelli, F. Baletto, R. Ferrando, Phys. Rev. Lett. **93**, 105503 (2004)
7. S. Darby, T.V. Jones, R.L. Johnston, C. Roberts, J. Chem. Phys. **116**, 1536 (2002)
8. A. Aguado, L.E. Gonzalez, J.M. Lopez, J. Phys. Chem. B **108**, 11722 (2004)
9. C. Mottet, G. Rossi, F. Baletto, R. Ferrando, Phys. Rev. Lett. **95**, 035501 (2005)
10. F. Baletto, C. Mottet, R. Ferrando1, Phys. Rev. Lett. **90**, 135504 (2003)
11. J. Bai, J.P. Wang, Appl. Phys. Lett. **87**, 152502 (2005)
12. S. Koutsopoulos, K.M. Eriksen, R. Fehrmann, J. Catal. **238**, 270 (2006)
13. F. Ding, A. Rosen, K. Bolton, Phys. Rev. B **70**, 075416 (2004)
14. R. Birringer, Mater. Sci. Eng. A **117**, 33 (1989)
15. R. Hultgren, P.D. Desai, D.T. Hawkins, M. Gleiser, K.K. Kelley, *Selected Values of the Thermodynamic Properties of Binary Alloys* (Metals Park, Ohio, 1973)

16. J. Luo, M.M. Maye, V. Petkov, N.N. Kariuki, L. Wang, P. Njoki, D. Mott, Y. Lin, C.J. Zhong, Chem. Mater. **17**, 3086 (2005)
17. T. Shibata, B.A. Bunker, Z. Zhang, D. Meisel, C.F. Vardeman II, J.D. Gezelter, J. Am. Chem. Soc. **124**, 11989 (2002)
18. H.G. Boyen, A. Ethirajan, G. Kastle, F. Weigl, P. Ziemann, Phys. Rev. Lett. **94**, 016804 (2005)
19. A. Christensen, P. Stoltze, J.K. Norskov, J. Phys.: Condens. Matter **7**, 1047 (1995)
20. L.H. Liang, G.W. Yang, B. Li, J. Phys. Chem. B **109**, 16081 (2005)
21. J.Y. Yang, W.Y. Hu, H.Q. Deng, D.L. Zhao, Surf. Sci. **572**, 439 (2004)
22. W.R. Wu, W.Y. Hu, S.C. Han, J. Alloy Comp. **420**, 83 (2006)
23. R.A. Johnson, Phys. Rev. B **41**, 9717 (1990)
24. I.A. Abrikosov, H.L. Skriver, Phys. Rev. B **47**, 16532 (1993)
25. F.R. de Boer, R. Boom, W.C.M. Mattens, A.R. Miedema, A.N. Niessen, *Cohesion in Metals* (North-Holland, Amsterdam, 1988)
26. H.J. Schaller, Z. Metallkde **70**, 354 (1979)
27. T.T. Tsong, Y.S. Ng, S.B. McLand Jr, J. Chem. Phys. **73**, 1464 (1980)
28. W. Hu, S. Xiao, J. Yang, Z. Zhang, Eur. Phys. J. B **45**, 547 (2005)
29. K.K. Nanda, S.N. Sahu, S.N. Behera, Phys. Rev. A **66**, 013208 (2002)
30. S.K.R.S. Sankaranarayanan, V.R. Bhethanabotla, B. Joseph, Phys. Rev. B **71**, 195415 (2005)